Deformation monitoring of a super-tall structure using real-time strain data

Yong Xia[*1, 2], Peng Zhang[1], Yi-qing Ni[1], and Hong-ping Zhu[2]

[1] *Department of Civil and Environmental Engineering, The Hong Kong Polytechnic University, Hong Kong, China*

[2] *School of Civil Engineering & Mechanics, Huazhong University of Science and Technology, Wuhan, Hubei, China*

**Corresponding author, Tel.: +852 2766 6066, Email:ceyxia@polyu.edu.hk*

ABSTRACT

Monitoring deformation of super-tall structures under different environmental conditions is an important and challenging issue in assessing the safety and serviceability of structures. This paper presents a new method for calculating structural deformation using real-time strain data, which can be easily measured at different sections. Assuming the structural deformation is of bending beam type, the deformation of the structure is associated with longitudinal strain. Virtual work theory is then used to calculate the horizontal displacement and tilt angle of the building on the basis of the strain data at different heights of the structure. The proposed method is applied to the 600 m tall Canton Tower (previously known as Guangzhou New TV Tower), on which a long-term structural health monitoring system including over 400 vibrating strain gauges has been installed at different heights. The displacements and tilts of the structure top under normal and typhoon conditions are calculated using real-time monitoring strain data. The calculated deformations show good agreement with the measurements by using global positioning system (GPS) and inclinometers. The temperature-induced maximum daily movement is similar to the value of typhoon-induced motion. Moreover, the displacement mode of the super-tall structure is also calculated and shows the bending type. Error analysis demonstrates that the calculated displacements have higher accuracy than the GPS-measured counterparts, and that the calculated tilts have similar accuracy as those measured by an inclinometer.

KEY WORDS: Structural health monitoring (SHM); super-tall structures; deformation; temperature

1. Introduction

In recent decades, numerous super-tall structures have been built in several modern cities worldwide, and a great number of such structures are still being constructed. Temperature-, wind-, and earthquake-induced lateral motions are some of the major concerns for such slender and flexible super-tall structures. Lateral displacement is a critical parameter for assessing the safety and serviceability of these buildings. In contrast to acceleration measurement, accurately measuring displacement in practice can be challenging. Although displacement can be calculated from the double integral of acceleration, the displacement may drift over time because of the static and low-frequency components of the measured acceleration data [1].

Recently developed advanced techniques have allowed the displacement measurement of large-scale structures. These techniques include the utilization of global positioning system (GPS), total station, radar, laser, and video camera. Except for GPS, these land-surveying techniques are often used for short-term monitoring rather than continuous long-term monitoring because such tools rely on good weather conditions and manpower. By contrast, GPS can automatically measure both static and dynamic deformations for a long period regardless of visibility or weather. Therefore, GPS is widely applied in measuring the deformations of civil structures, such as long-span bridges [2–6], high-rise buildings [7–14], and dams [15–16]. A number of studies integrated the GPS with other conventional instruments, such as accelerometers [17–19], robotic total stations [20], and inclination sensors [21] to enhance the accuracy of measurement. Nevertheless, GPS accuracy in practice is still not very high. The quality of GPS measurement can be affected by various factors, such as satellite visibility, availability and geometry, quality of signal sent, delays caused by GPS waves crossing the ionosphere and troposphere, and multipath [22].

This study presents a new method for calculating the deformation of super-tall structures based on the assumption that the entire structure can be regarded as a cantilever beam. Thus, the deformation of the beam can be associated with the strain. Consequently, the displacement and tilt can be calculated from the strain using virtual work theory. The effectiveness of the technique is verified through its application to the Canton Tower, on which a long-term health monitoring system has been installed [23–26]. The calculated displacements and tilts under different environmental conditions are compared with those measured using GPS and inclinometer. In addition, the displacement profile of the structure along the height can be obtained as well, which is not available using other approaches.

2. Canton Tower and its SHM system

2.1. Canton Tower

The Canton Tower (previously known as Guangzhou New TV Tower) is a concrete–steel composite structure (Fig. 1) that consists of a main tower (454 m tall) and an antennary mast (146 m tall). The main tower is a tube-in-tube structure. As shown in Fig. 2, the inner tube has an oval shape with a constant dimension of 14 m × 17 m. The long axis of the inner tube is directed toward of 18° west to north. The outer frame tube consists of 24 concrete-filled-tube (CFT) columns, which are uniformly spaced in an oval, inclined in the vertical direction, and connected by hollow steel rings and braces. The dimension of the oval decreases from 50 m × 80 m at the underground level to a minimum of 20.65 m × 27.5 m at the height of 280 m and then increases to 40.5 m × 54 m at the top of the tube (454 m). The CFT columns are linked by 46 steel ‘ring’ beams at an inclination angle of 15.5° to the horizontal plane. The hollow steel braces connect all of the joints of the CFT columns and ring beams. It can be seen that the floor is not directly attached to the outer tube. The radiating steel girders in the floor stretch out from the bottom of the floor and are connected to the corresponding CFTs of the outer tube through a bolt in the CFT.

Fig. 1 Perspective view of the Canton Tower

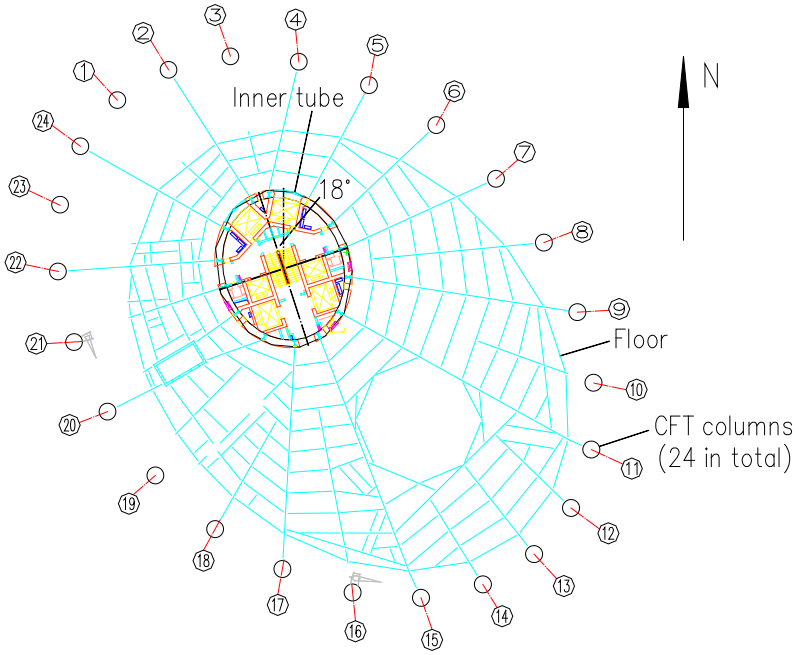

Fig. 2 A typical floor plan of Canton Tower

2.2. SHM system for Canton Tower

A long-term structural health monitoring (SHM) system was implemented on the Canton Tower by a team from The Hong Kong Polytechnic University and Sun Yat-sen University. The SHM system, which consists of 16 different types of over 800 sensors, employs a pioneering SHM practice that integrates in-construction monitoring and in-service monitoring [23−25]. The strain and temperature monitoring subsystem employed during the construction stage consisted of vibrating wire strain gauges, thermal sensors, and substations distributed along 12 sections at different heights. As shown in Fig. 3, the elevations of 32.8, 100.4, 121.2, 173.2, 204.4, 230.4, 272.0, 303.2, 334.4, 355.2, 386.4, and 438.4 m were chosen as the 12 critical sections for the concrete inner structure. These elevations corresponded to Ring Nos. 3, 9, 11, 17, 21, 24, 28, 32, 35, 38, 40, and 45 of the outer tubular structure. The data on each section are collected by the corresponding substations and then transmitted to a control room.

Four points (denoted as Points 1 to 4 in Fig. 4) at each critical section of the inner tube are installed with a 45° strain rosette, each consisting of three Geokon vibrating wire strain gauges [27] to measure the strain of the concrete wall. The temperature of the points is measured by the thermistor embedded in the vibrating wire. The SHM project was started in June 2007 when the inner tube has been constructed to the height of approximately 120 m. The section at 121.2 m was equipped with gauges embedded inside the inner core wall. The sensors for the sections above 121.2 m were then embedded inside the wall as the construction progressed, whereas those for the sections at 32.8 and 100.4 m were installed on the exterior surface of the core wall [28] because the concrete construction had been completed by that time. The gauges at these two sections were attached to two grouted concrete mounting blocks on the wall.

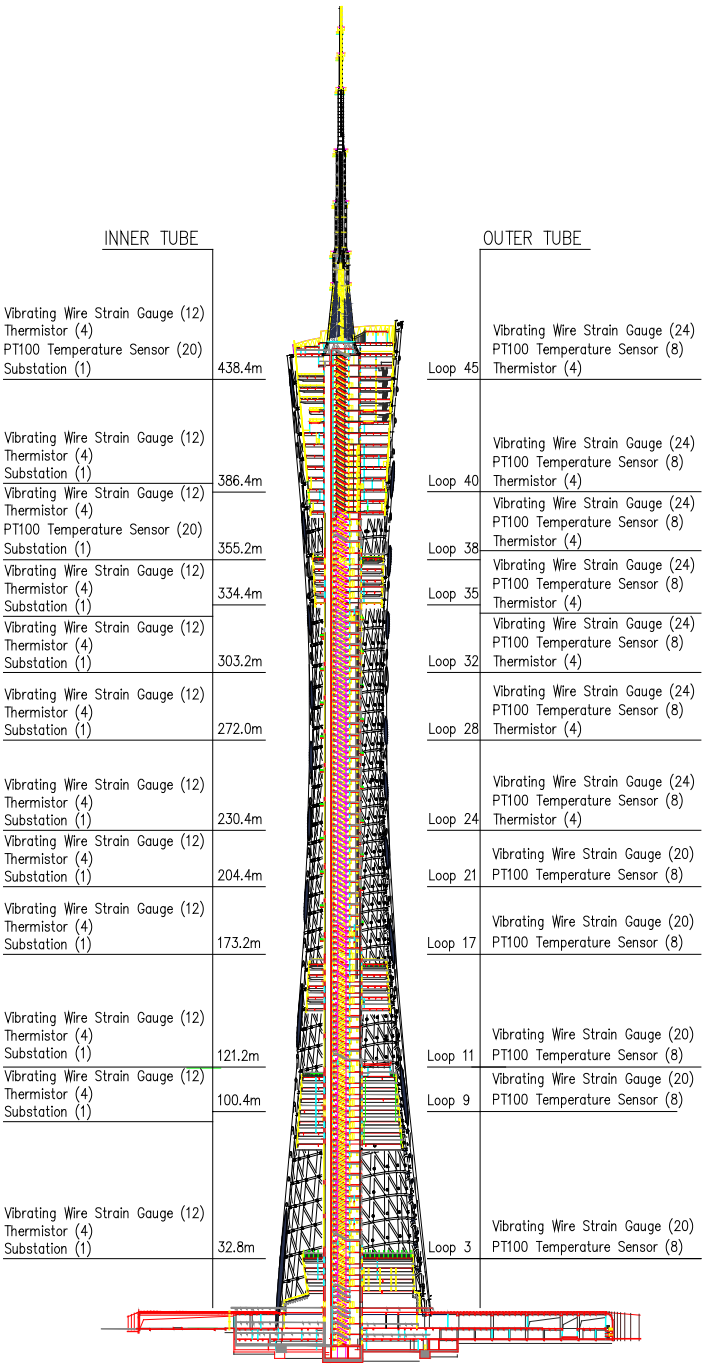

Fig. 3 Layout of the strain and temperature monitoring subsystem

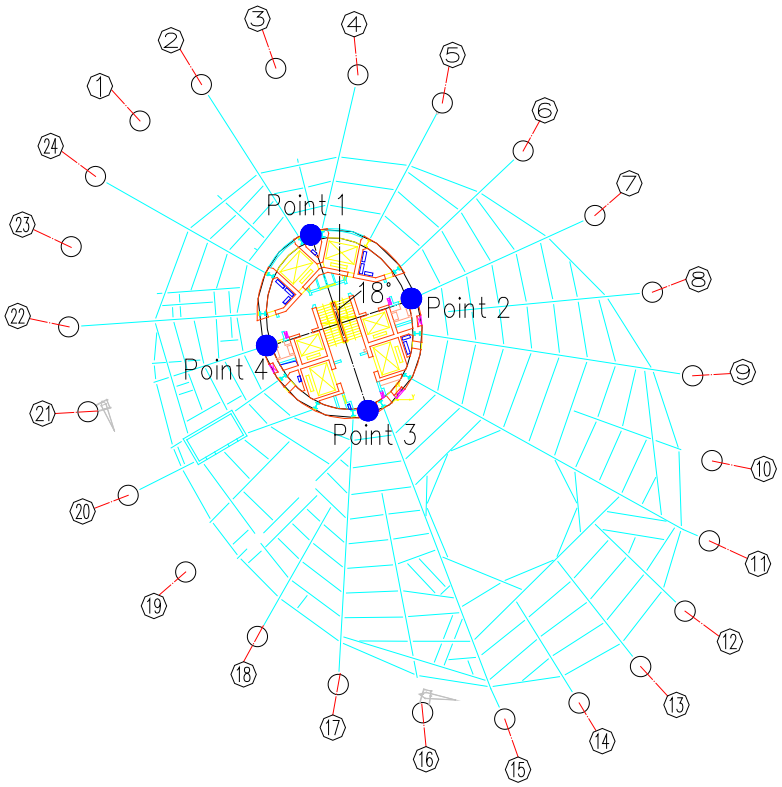

Fig.4 Location of strain and temperature monitoring points at one critical section

A GPS system was installed to monitor the displacement of the Canton Tower. The reference station (Fig. 5(a)) was installed 3 m above the sightseeing platform at 10.2 m. The rover station (Fig. 5(b)) was installed over a chimney at approximately 6 m above the platform at 459.2 m. In addition, a Leica Nivel 210 inclinometer (Fig. 6) was installed at the height of 443.8 m to measure the tilt angles (or inclination from the horizontal) along the short and long axes of the inner tube. The sampling rate of the GPS and inclinometer was set to 1 Hz.

(a) Reference station (b) Rover station

Fig. 5 GPS installed on the structure

Fig. 6 Inclinometer installed on the structure

3. Derivation of deformation using the measured strain data

For slender and flexible super-tall structures that stand hundreds of meters, the tube can be regarded as a cantilever beam. The deformation of the cantilever beam can be represented by the longitudinal strain at different sections. As illustrated in Fig. 7(a), a deformed cantilever beam is divided into *n* segments according to the available strain measurement points. The

length of the *i*-th segment is h_i. At point *i*, the strain difference across the section is $\Delta\varepsilon_i$. If the strain difference between the measurement points is assumed to vary linearly, then the strain difference distribution along the entire beam can be shown as Fig. 7(b). Fig. 7(c) shows the deformation of an infinitesimal element of length *dh*. The angular rotation of the infinitesimal element can be expressed as follows:

$$d\theta = \frac{(\varepsilon_l - \varepsilon_r)dh}{b} = \frac{\Delta\varepsilon dh}{b} \tag{1}$$

where ε_l and ε_r are the vertical strain at the left and right surfaces of the element, respectively, $\Delta\varepsilon$ is their difference, and *b* is the height of the section.

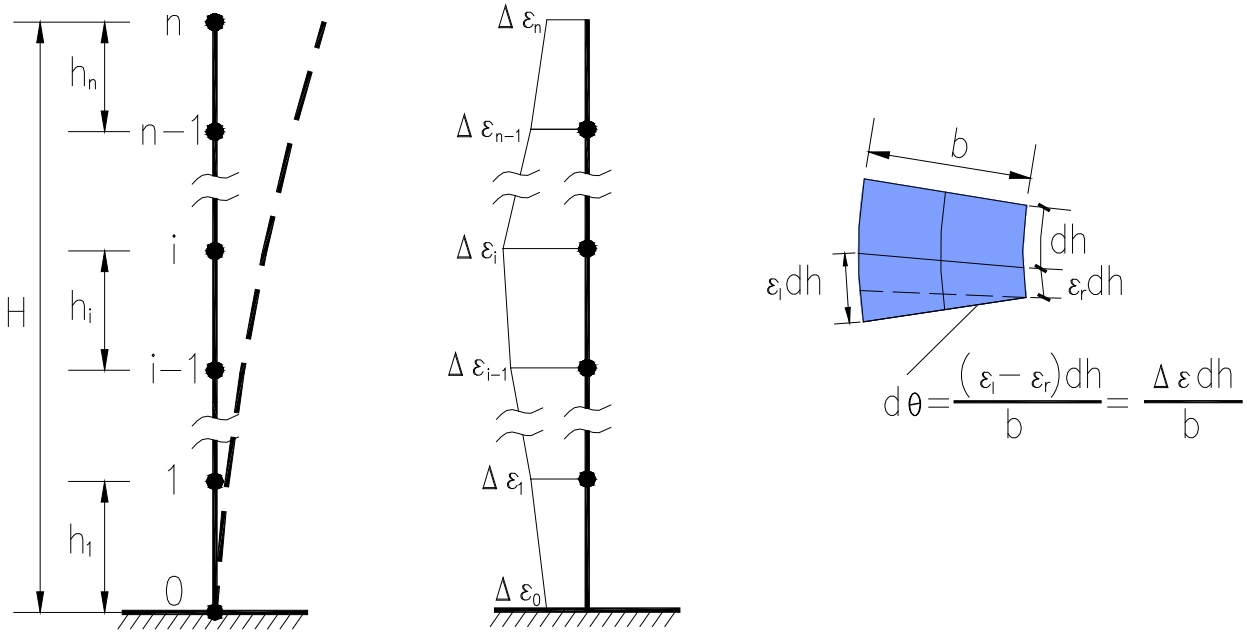

(a) Cantilever beam (b) Strain distribution (c) Deformation of an infinitesimal element

Fig. 7 Deformed cantilever beam

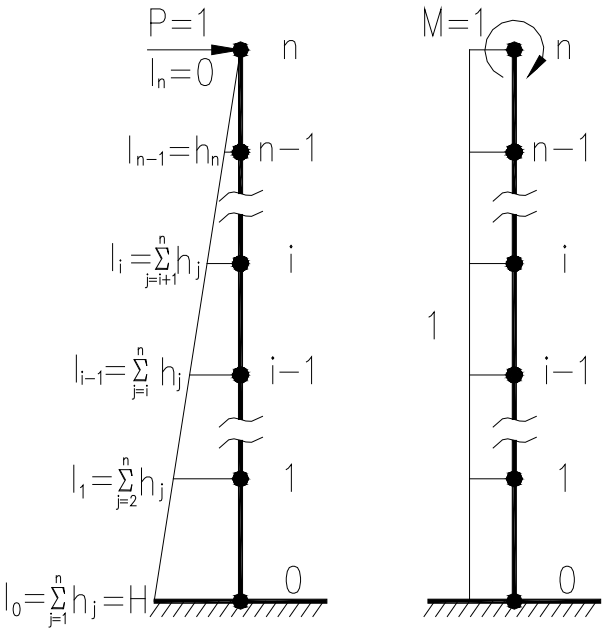

(a) Unit force (b) Unit moment

Fig. 8 Bending moment diagram (M_u) of the beam subject to a unit virtual force

A unit virtual force is horizontally applied at point *n* to calculate the horizontal displacement at the top of the beam. The resulting bending moment (M_u) is plotted in Fig. 8(a). The bending moment at point *i* is

$$l_i = \sum_{j=i+1}^{n} h_j \qquad (i = 0 \sim n-1) \tag{2}$$

$$l_n = 0 \tag{3}$$

According to the virtual work theory, the displacement at the top of the beam in Fig. 7(a) can be calculated as follows:

$$v_n = \int M_u d\theta = \frac{1}{b}\int_0^H M_u \Delta\varepsilon dh \tag{4}$$

Integration of Eq. (4) can be calculated using the moment diagram multiplication method:

$$v_n = \frac{1}{6b}\sum_{i=1}^{n}[h_i(2l_{i-1}\Delta\varepsilon_{i-1} + l_{i-1}\Delta\varepsilon_i + l_i\Delta\varepsilon_{i-1} + 2l_i\Delta\varepsilon_i)] \tag{5}$$

Therefore, the top horizontal displacement can be calculated from the strain at different heights.

Similarly, a unit virtual moment is applied at point *n* to calculate the tilt (or inclination) at the top of the beam. The resulting bending moment is shown in Fig. 8 (b). Therefore, the tilt angle can be calculated as follows:

$$\theta_n = \int M_u d\theta = \frac{1}{b}\int_0^H M_u \Delta\varepsilon dh = \frac{1}{2b}\sum_{i=1}^{n}(\Delta\varepsilon_{i-1} + \Delta\varepsilon_i)h_i \quad (6)$$

With regarding to the Canton Tower, the vertical strains of the four measuring points at each section in the inner tube are available. Among the 12 critical sections of the inner tube, the strain data measured by the surface-type sensors installed at sections 32.8 and 100.4 m are rather noisy and are therefore disregarded in calculating the deformation of the tower; only the strain data from the ten sections above 100.4 m will be used. The inner tube is then divided to 11 segments (n = 11). According to Eqs. (5) and (6), the horizontal displacement and tilts along the short and long axis directions of the tower top can be calculated using the measured strain data at each time instance. In particular, the measurements of points 2 and 4 at these sections are used to calculate the deformation along the short axis direction, and those of points 1 and 3 are used to calculate the deformation along the long axis direction. Given that point 0 has not been measured, the strain data at point 1 will be used instead, i.e., $\Delta\varepsilon_0 = \Delta\varepsilon_1$. Similarly, $\Delta\varepsilon_{11} = \Delta\varepsilon_{10}$ as the strain at the top of the structure is not available.

4. Comparison between calculated and measured deformation

To verify the effectiveness of the proposed method, the horizontal displacement and tilt of the tower top derived from the strain data are respectively compared with the measurements using GPS and inclinometer. Considering that the GPS output results are in the east and north directions, the derived displacements are transformed according to the following equation:

$$\begin{bmatrix} X_d' \\ Y_d' \end{bmatrix} = \begin{bmatrix} \cos\alpha & -\sin\alpha \\ \sin\alpha & \cos\alpha \end{bmatrix} \begin{bmatrix} X_d \\ Y_d \end{bmatrix} \quad (7)$$

As shown in Fig. 9, X_d and Y_d are displacements along the short and long axes, respectively; X_d' and Y_d' are displacements to the east and north, respectively; and α is the angle between the long axis and the north.

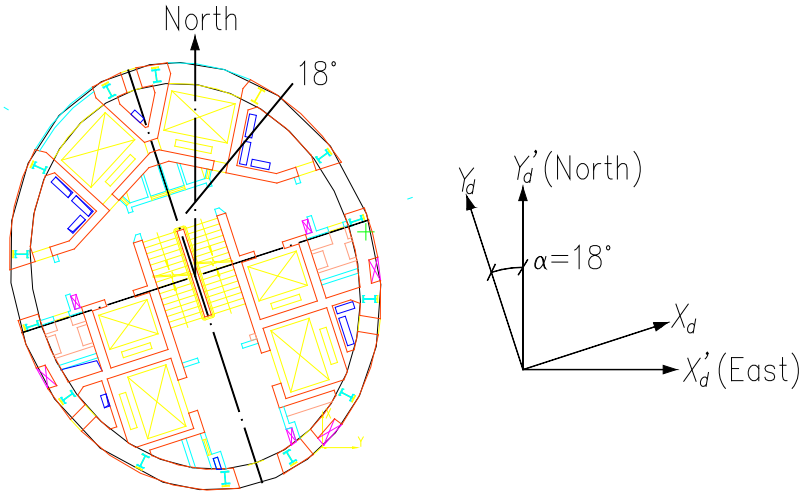

Fig. 9 Plan view of coordinate transformation

4.1. Temperature and typhoon-induced displacement

4.1.1. One typical sunny day

During sunny days with low wind speed, the deformation of the structure is mainly induced by the temperature variation because there is no other significant loading on the structure. Fig. 10 shows the air temperature on 3 December 2008, which was a day when the wind speed was low. Fig 11 shows the relative vertical strain variation of the four measurement points at section 121.2 m during the day. Here the strain at midnight (00:00) is set as the initial reference value, with the results calculated at later times indicating relative changes to the reference values. This method is utilized because the actual position of the tower is unknown. The strain at point 2 (east) increased first at approximately 7:00. Subsequently, the strain at points 3, 4, and 1 increased at approximately 8:00, 12:00, and 14:00, respectively. The maximum strain difference between points 2 and 4 was approximately 15 με, whereas that between points 1 and 3 was approximately 10 με.

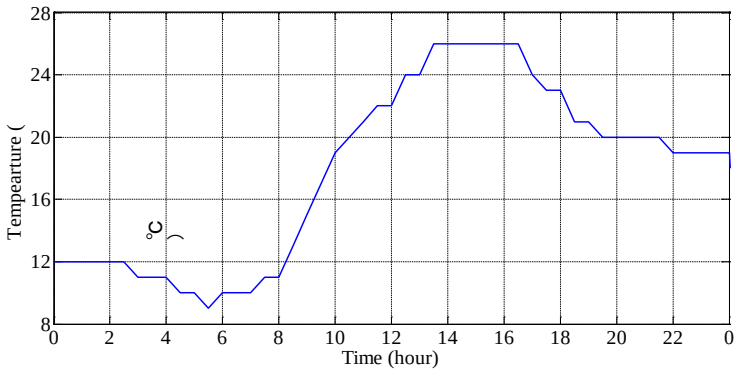

Fig. 10 Air temperature in Guangzhou on 3 December 2008

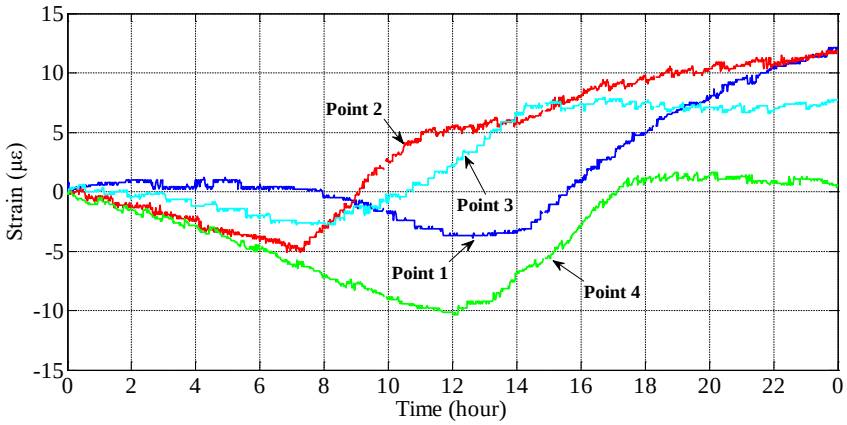

Fig. 11 Relative strain at section 121.2 m on 3 December 2008

By using the measured strain data at 10 different sections, the displacement of the tower top in the east and north directions on 3 December 2008 is calculated and compared with the GPS measurements, as shown in Fig. 12. The GPS data have a higher sampling frequency compared with that of the strain gauges. Thus, the former were resampled by averaging the data to the same frequency as the latter and then smoothed using the five-point moving average algorithm [29]. The derived and measured displacement data exhibited the same variation trend. The maximum displacement toward the west and north directions occurred at almost the same time. In particular, the GPS-measured maximum motion was 9.1 cm in the east–west direction and 10.7 cm in the south–north; the corresponding derived values were 11.4 and 8.8 cm.

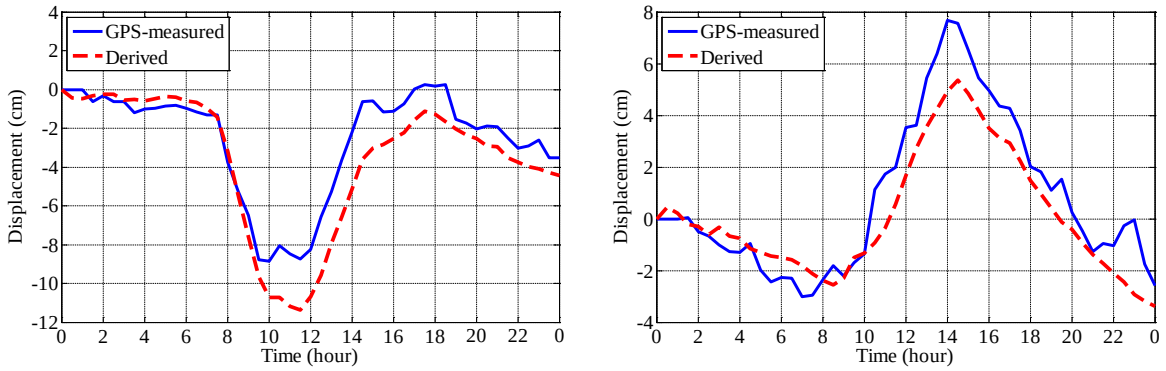

(a) East direction (b) North direction

Fig.12 Comparison between GPS-measured and derived displacements at the top of the inner structure on 3 December 2008

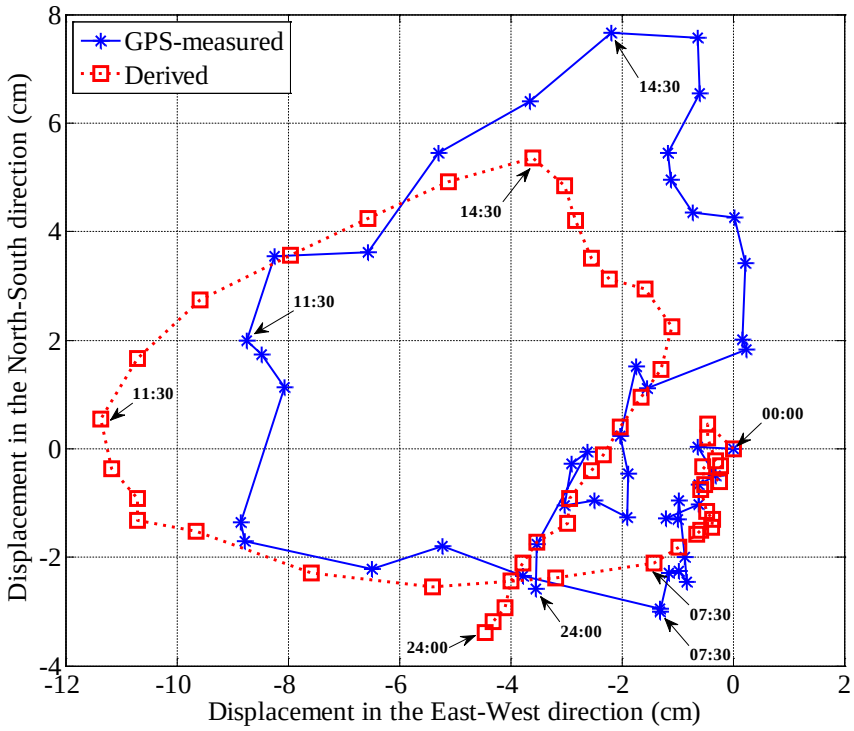

Fig. 13 Derived and measured displacement track at the top of the inner structure on 3 December 2008

Fig. 13 shows the daily movement track at an interval of 0.5 hour. The positions were averaged from the data every half-hour period. Both curves start at 00:00 am from the origin to allow comparison. Both curves exhibit similar moving patterns. The members of the tower that are exposed to the sun received direct solar radiation. Thus, these members had higher temperatures compared with those on the shaded facade, causing the structure to bend away from the sun. During early mornings (before 7:00), the movement of the tower was small and

slow. After sunrise, the tower started to move toward west and arrived to its westernmost position at approximately 11:30. When the sun moved to the west in the afternoon, the temperature of the members in the southwest increased, causing the tower to move northeast. At 14:30, the tower reached its northernmost position. Afterward, the temperature difference among the tower members decreased, causing the tower to move back gradually from the north to the south.

4.1.2. One month displacement

During the in-service monitoring period, the GPS was installed and operated permanently to monitor the displacement of the tower top for a long-term period. The air temperature variation in April 2013 approximately ranged from 12 °C to 31 °C, as illustrated in Fig. 14. No heavy wind or typhoon occurred during this month. Thus, the deformation of the tower can be primarily attributed to temperature. For this month, the maximum daily temperature difference, which ranged from 18 °C to 30 °C, occurred on 15 April 2013.

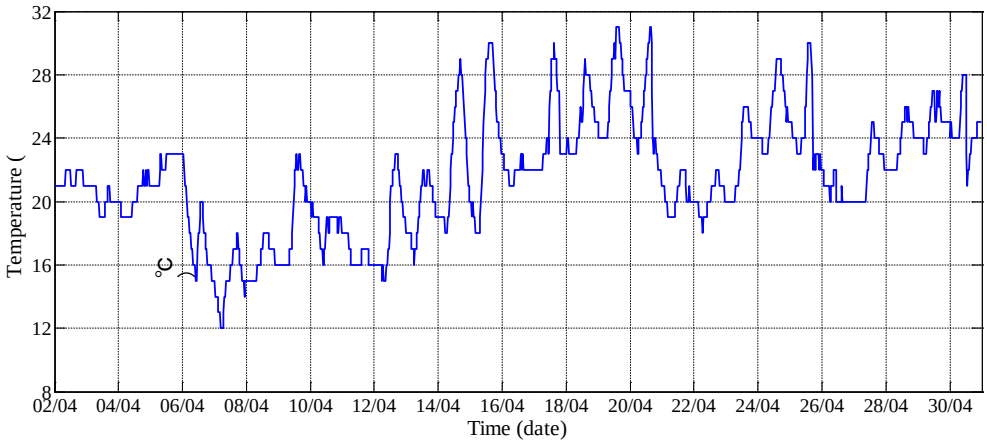

Fig. 14 Air temperature in Guangzhou in April 2013

The derived and GPS-measured tower top displacement in the east and north directions during April 2013 are compared in Figs. 15 and 16, respectively. The two sets of displacement data exhibit similar variation trend, although a number of discrepancies exist. Most days in April were rainy or cloudy except the 12th, 14th, and 15th. The displacement variations in these three sunny days were much larger than other days. The maximum GPS-measured daily motion

during sunny days was 16.1 cm in the east–west direction and 7.4 cm in the south–north; the corresponding derived values were 12.1 and 7.4 cm. The GPS-measured and derived displacement variations during rainy and cloudy days were quite small, that is, less than 6 cm in the east direction and 4 cm in the north. The GPS-measured peak-to-peak motion for the entire month was 18.7 cm in the east–west direction and 12.1 cm in the south–north; the corresponding derived counterparts were 16.3 and 12.1 cm.

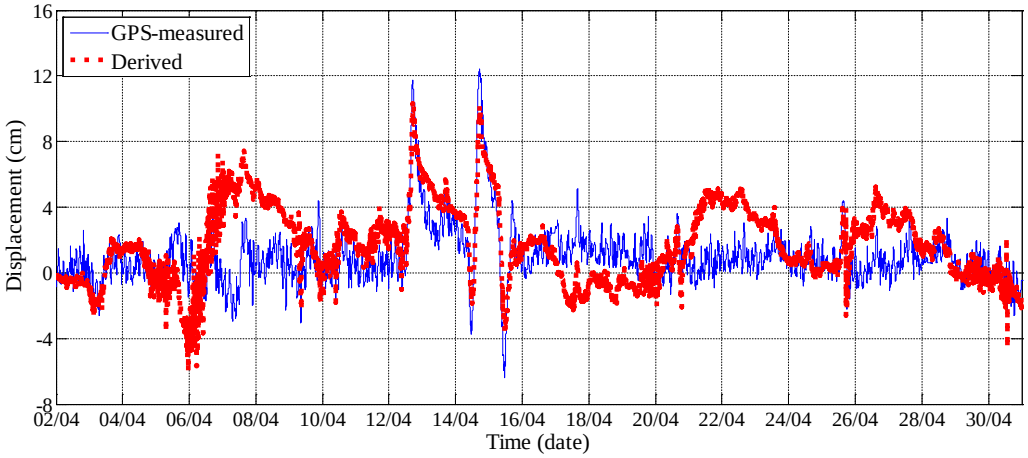

Fig. 15 Comparison between GPS-measured and derived displacements at the top of the inner structure in April 2013 (east direction)

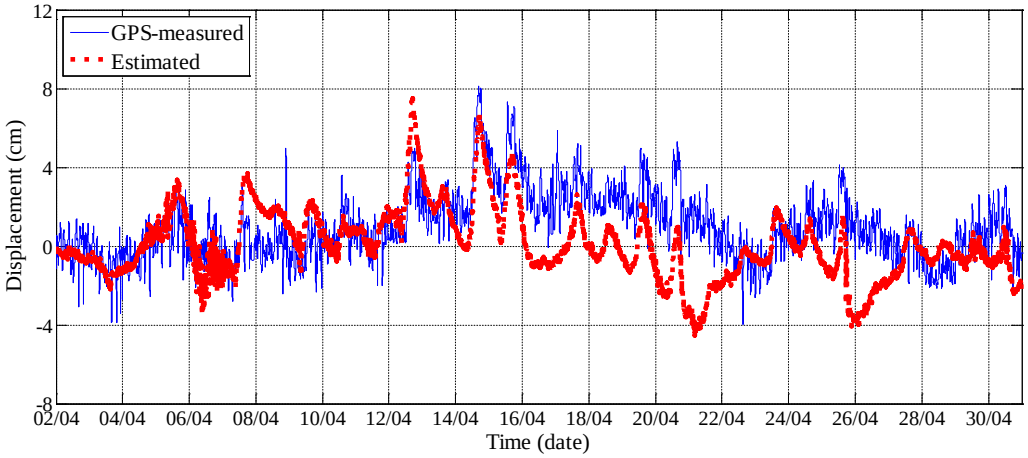

Fig. 16 Comparison between GPS-measured and derived displacements at the top of the inner structure in April 2013 (north direction)

4.1.3. Typhoon period

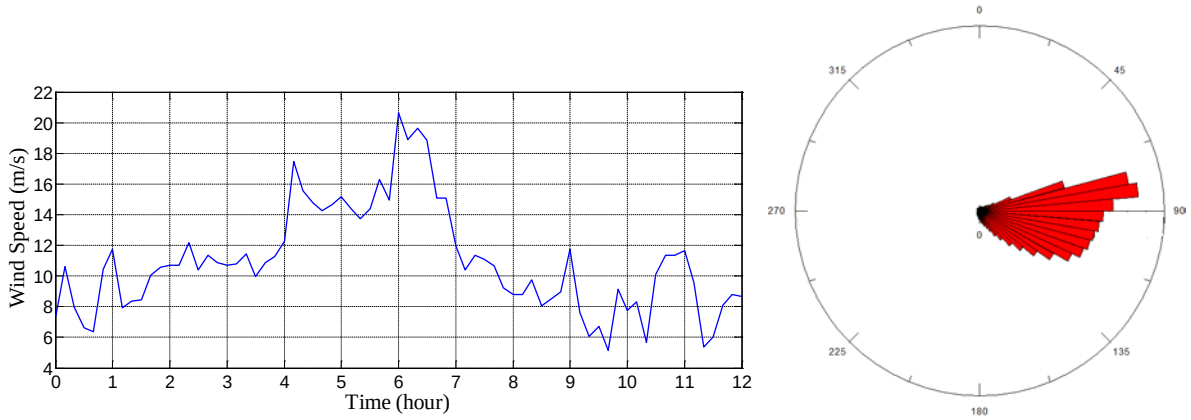

Fig. 17 Ten-minute mean wind speed at the top of the tower (left) and wind rose diagram (right) on 15 September 2009 during Typhoon Koppu

The Canton Tower is located in a typhoon-prone region and is thus subject to several typhoon incidents each year. Typhoon Koppu struck Guangdong Province from 14 September to 15 September in 2009. Fig. 17 shows the 10-minute mean wind speed, which was measured by the anemometer installed on the top of the tower. The maximum mean wind speed was 20.9 m/s, which occurred approximately between 6:00 to 7:00. The wind speed direction was mainly toward the west. Figs. 18 and 19 present the comparisons of the derived and measured displacements during this typhoon incident from 19:00 on 14 September to 10:00 on 15 September. The derived displacement exhibited the same pattern as that of the GPS-measured displacement. The maximum displacement in the west direction occurred between 6:00 to 7:00 on 15 September when the wind speed was at its maximum. The GPS-measured peak-to-peak motion was 15.2 cm in the east–west direction and 8.1 cm in the south–north; the corresponding calculated counterparts were 15.3 and 8.4 cm. These measurements are similar to the daily temperature-induced displacements.

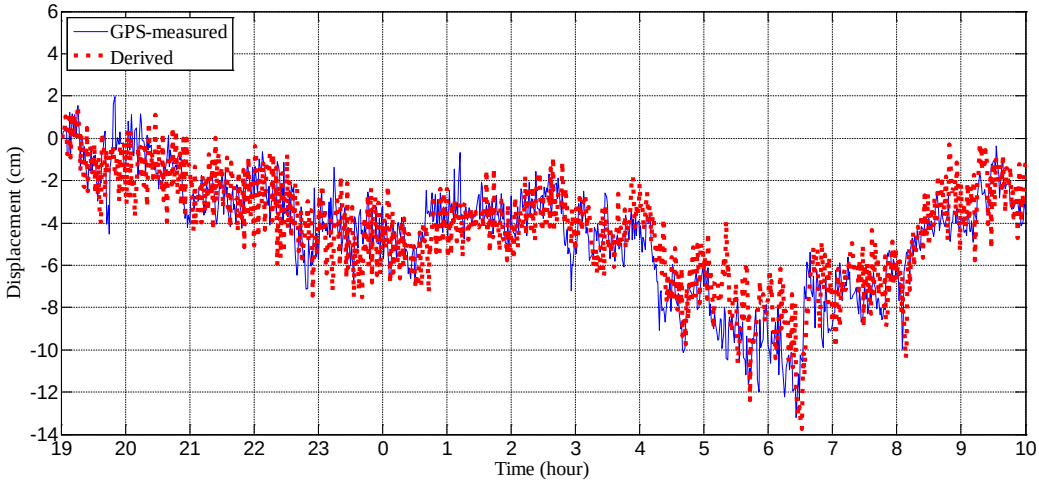

Fig. 18 Derived and measured typhoon-induced displacement at top of the Tower (east direction)

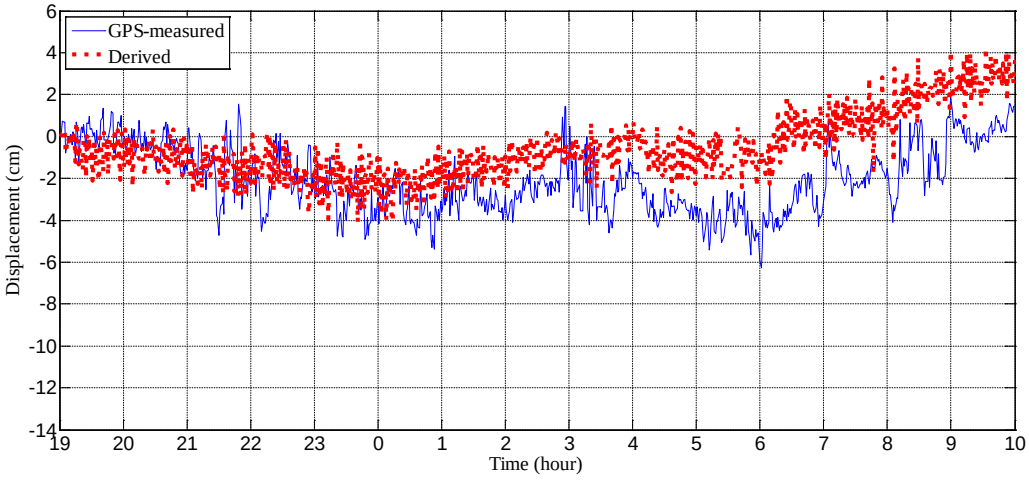

Fig. 19 Derived and measured typhoon-induced displacement at top of the Tower (north direction)

4.2. Comparison between calculated and inclinometer-measured tilt

Both the derived and inclinometer-measured tilts are along the long and short axes of the inner tube. Thus, coordinate transformation is no longer necessary, and the two results can be compared directly. The sampling rate of the inclinometer was 1 Hz. Thus, the measured tilt data are resampled by averaging the data in one minute.

Fig. 20 compares the measured and derived tilt at the height of 443.4 m on 15 August 2011, which was a typical sunny day. The tilt angle is positive when the tower moves to the southwest

along the short axis or to the southeast along the long axis. The air temperature on this day ranged from 27 °C to 36 °C, as shown in Fig. 21. As shown in Fig. 20, the two tilt curves exhibit good agreement, although a number of discrepancies can be found along the long axis. During early morning (before 6:00), the tilt angle had little change. After the sun rose from the southeast, the structural temperatures in the southeast became higher compared with that on the opposite side. The tower bent to the northwest, resulting in an increase in the tilt angle along the short axis and a decrease along the long axis. During the afternoon, the sun moved to the southwest. The structural temperatures in the southwest facade began to rise, causing the tower to move back. The tilt angle along the short axis decreased, whereas that along the long axis increased. The temperature differences between the members on different facades were similar during midnight, and the tower almost moved back to its original location. The measured peak-to-peak tilt angle was 0.82 mrad along the short axis and 0.18 mrad along the long axis; the corresponding derived counterparts were 0.66 and 0.21 mrad.

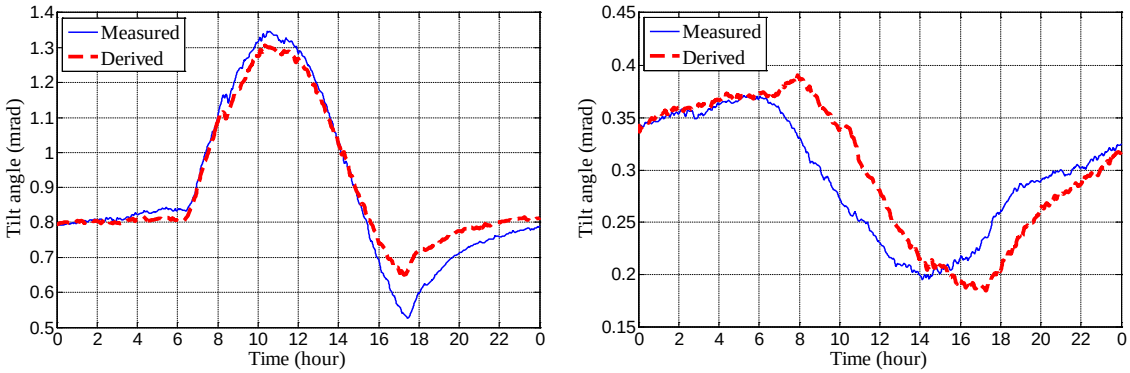

(a) short axis (b) long axis

Fig. 20 Derived and measured tilts at the height of 443.4 m of the tower on 15 August 2011

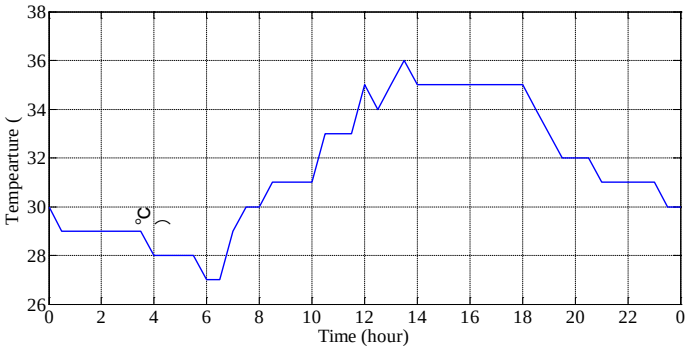

Fig. 21 Air temperature in Guangzhou on 15 August 2011

Fig. 22 compares the measured and derived tilts at the height of 443.4 m on 14 December 2011. The air temperature on this day ranged from 10 °C to 23 °C. Similarly the tilt angle along the short axis increased in the morning till to 10:00, decreased afterwards, and increased again after 17:00. The measured and derived tilts generally agree well. The tilt angle along the long axis was relatively small.

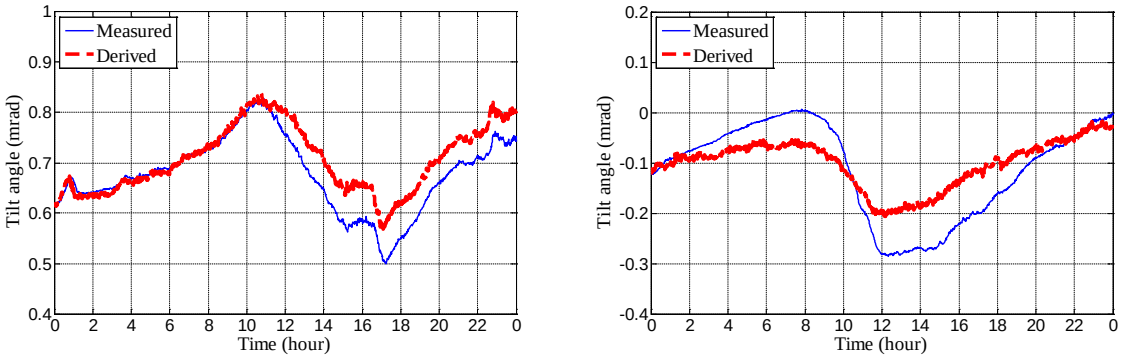

(a) short axis (b) long axis

Fig. 22 Derived and measured tilts at the height of 443.4 m of the tower on 14 December 2011

5. Displacement mode of the Canton Tower

The above procedure of calculating the deformation at the top of the structure can also be applied to calculating the deformation at other floors by applying the unit virtual force at the corresponding points. By this approach, the deformation mode, or deformation profile of the entire structure along the height can be derived. This is another advantage of the present technique. As the strain measurements are available at 11 floors only, the strain data at other floors are interpolated. Fig. 23 plots the displacement profile of the Tower at 11:30 on 3 December 2008, when the Tower had the maximum horizontal east-west displacement (see Fig. 13). The south-north displacement was small and not shown here. The deformation showed the bending mode of the entire structure, different from the bending-shear mode of a typical frame−wall structure. This is because the floors of the Canton Tower are not attached to the outer tube and the floor girders are connected to the outer frame columns through bolts. Such a joint design causes the CFT columns can rotate freely to release the bending moment of the joints. Consequently the outer frame tube has less restraint on the deformation of the inner tube.

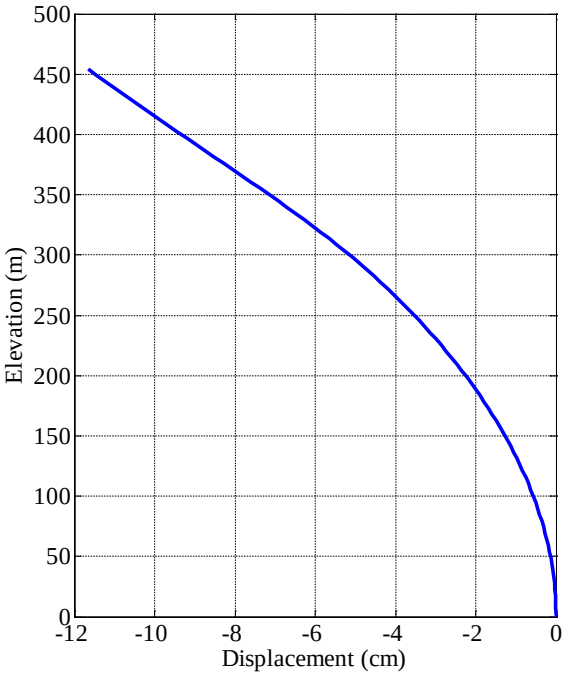

Fig. 23 East-west displacement profile of the Tower along the height at 11:30 on 3 December 2008

6. Error analysis

The derived deformation of the structure is subject to uncertainty because the strain measurements contain noise. The accuracy of the derivation depends on two factors. One factor is the beam bending model used in this paper. The assumption of the bending-type deformation can be accepted because the length-to-depth ratio of the main tower is approximately 26.7. The other source of uncertainty is measurement error. Based on Eqs. (5) and (6), the uncertainties of the derived displacement and tilt depend on the measurement error of the strain because the length and section height of each segment could be known accurately. The standard deviation of a multivariate function $y=f(x_1, x_2,\ldots\ldots x_n)$ can be expressed as follows:

$$\sigma_y = \sqrt{(\frac{\partial y}{\partial x_1})^2 \sigma_{x_1}^2 + (\frac{\partial y}{\partial x_2})^2 \sigma_{x_2}^2 + \cdots\cdots + (\frac{\partial y}{\partial x_n})^2 \sigma_{x_n}^2} \qquad (8)$$

where variables x_i $(i = 1, 2, \ldots, n)$ are independent to each other, and σ is the standard deviation.

By applying Eq. (8) to Eq. (5), the standard deviation of the derived displacement at the top can be expressed as follows:

$$\sigma_{v_n} = \frac{1}{6b}\sqrt{h_1^2(2l_0 + l_1)^2\sigma_{\Delta\varepsilon_0}^2 + \sum_{i=1}^{n-1}[h_i(l_{i-1} + 2l_i) + h_{i+1}(2l_i + l_{i+1})]^2\sigma_{\Delta\varepsilon_i}^2 + h_n^2(l_{n-1} + 2l_n)^2\sigma_{\Delta\varepsilon_n}^2} \quad (9)$$

Similarly, the standard deviation of the tilt at the top can be calculated as follows:

$$\sigma_{\theta_n} = \frac{1}{2b}\sqrt{h_1^2\sigma_{\Delta\varepsilon_0}^2 + \sum_{i=1}^{n-1}(h_i + h_{i+1})^2\sigma_{\Delta\varepsilon_i}^2 + h_n^2\sigma_{\Delta\varepsilon_n}^2} \quad (10)$$

In the long axis,

$$\sigma_{\Delta\varepsilon_i}^2 = \sigma_{\varepsilon_{i1}}^2 + \sigma_{\varepsilon_{i3}}^2 \quad (11)$$

where $\sigma_{\varepsilon_{i1}}$ and $\sigma_{\varepsilon_{i3}}$ are the standard deviations of the measured strain at points 1 and 3 on the *i*-th section, respectively. Similarly in the short axis,

$$\sigma_{\Delta\varepsilon_i}^2 = \sigma_{\varepsilon_{i2}}^2 + \sigma_{\varepsilon_{i4}}^2 \quad (12)$$

where $\sigma_{\varepsilon_{i2}}$ and $\sigma_{\varepsilon_{i4}}$ are the standard deviations of the measured strain at points 2 and 4 on the *i*-th section, respectively.

The standard deviation of each strain sensor can be estimated from the measured strain data. During early morning, the temperatures of the structural members are almost stable and similar. During this period, if the wind speed is low and no special loading acts on the structure, the variation of the measured strain data can be mainly attributed to the measurement noise, and the standard deviation of each sensor can be calculated. The standard deviations of the strain measurements on 3 December 2008 are listed in Table 1. These measurements range from 0.3 με to 2.6 με, which coincide with the precision of the vibrating wires. If the different strain gauges are presumed to be independent, then the standard deviations of the derived displacements along the long and short axes can be respectively calculated as 0.29 and 0.31 cm according to Eq. (9). This uncertainty level is lower than that of the GPS measurements, which accuracy is generally regarded at the millimeter level under ideal laboratory conditions and a few centimeters under normal field measurement conditions because of numerous practical difficulties such as multipath [20, 30]. Therefore, the proposed strain-based displacement results can achieve higher accuracy compared with the GPS measurement results.

Similarly, the standard deviations of the derived tilt angles along the long and short axes can be respectively calculated as 0.0056 and 0.0084 mrad, according to Eq. (10). These calculated values are similar to the precision of the inclinometer, which has a nominal accuracy of ±0.01 mrad.

Table 1 Standard deviations of measured strain on 3 December 2008

Section No. (elevation)	Standard Deviation (με)			
	Point 1	Point 2	Point 3	Point 4
S3 (121.2 m)	0.27	0.83	1.44	0.96
S4 (173.2 m)	0.30	1.22	0.69	0.83
S5 (204.4 m)	1.27	0.56	0.24	0.75
S6 (230.4 m)	0.36	0.78	0.76	0.68
S7 (272.0 m)	0.75	0.97	1.65	1.56
S8 (303.4 m)	0.41	1.43	0.79	0.60
S9 (334.4 m)	0.84	0.35	0.32	1.47
S10 (355.2 m)	0.32	0.64	2.09	1.00
S11 (386.4 m)	0.44	0.39	1.54	2.58
S12 (438.4 m)	0.42	0.59	1.74	1.10

7. Conclusions

In this paper, distributed strain data obtained from an SHM system are employed to derive the displacement and tilt of super-tall towers. The derivation is based on the assumption that the inner tube is a bending type structure and that shear deformation can be ignored in the sections. The derived displacement and tilt are then compared with field monitoring data. Error analysis is conducted to investigate the accuracy of the proposed approach. The following conclusions are drawn:

1. The GPS-measured daily motion at the top of the Canton Tower during sunny days was about 16 cm in the east–west direction and 7 cm in the south–north; the corresponding derived values were 12 and 7 cm. The GPS-measured and derived displacement variations during rainy and cloudy days were less than 6 cm in the east–west direction and 4 cm in the south–north.
2. Comparison shows that the indirectly-derived horizontal displacement and tilt of the structure are in good agreement with the direct measurements using GPS and the

inclinometer. The proposed method can be an alternative technique for calculating the deformation of super-tall structures.

3. On a sunny day, the movement of the tower top's movement follows a west–north–east–south clockwise pattern. The temperature-induced maximum daily movement is similar to the typhoon-induced motion.
4. The deformation mode of the Canton Tower is also calculated and shows the bending deformation type. This is because the girder-frame joints are pin connected and thus, the frame effect of the entire structure is not as strong as a typical frame-wall system.
5. Error analysis shows that the derived displacement has higher accuracy than the GPS-measured results. In addition, the derived tilt has similar accuracy with the inclinometer-measured results.

Acknowledgements

The authors gratefully acknowledge the financial support provided by the National Natural Science Foundation of China (Project No. 51328802) and the Research Grants Council of the Hong Kong Special Administrative Region, China (Project No. PolyU 5285/12E).

References

[1] Chan WS, Xu YL, Ding XL, Dai WJ. An integrated GPS–accelerometer data processing technique for structural deformation monitoring. J Geodesy 2006; 80:705–19.

[2] Roberts GW, Meng XL, Dodson AH. Integrating a Global Positioning System and accelerometers to monitor the deflection of bridges. J Surv Eng, ASCE 2004; 130(2):65–72.

[3] Roberts GW, Cosser E, Meng XL, Dodson A. High frequency deflection monitoring of bridges by GPS. J Glob Position Syst 2004; 3(1–2):226–31.

[4] Meng XL, Dodson AH, Roberts GW. Detecting bridge dynamics with GPS and triaxial accelerometers. Eng Struct 2007; 29:3178-84.

[5] Xu YL, Chen B, Ng CL, Wong KY, Chan WY. Monitoring temperature effect on a long suspension bridge. Struct Control Hlth 2010; 17:632-53.

[6] Xia Y, Chen B, Zhou XQ, Xu YL. Field Monitoring and numerical analysis of Tsing Ma Suspension Bridge temperature behavior. Struct Control Hlth 2013; 20:560-75.

[7] Tamura Y, Matsui M, Pagnini LC, Ishibashi R, Yoshida A. Measurement of wind-induced response of buildings using RTK-GPS. J Wind Eng Ind Aerod 2002; 90(12–15):1783–93.

[8] Breuer P, Chmielewski T, Corski P, Konopk E. Application of GPS technology to measurements of displacements of high-rise structures due to weak winds. J Wind Eng Ind Aerod 2002; 90(3):223–30.

[9] Breuer P, Chmielewski T, Gorski P, Konopka E, Tarczynski L. The Stuttgart TV Tower—displacement of the top caused by the effects of sun and wind. Eng Struct 2008; 30(10):2771–81.

[10] Brownjohn JMW. Lateral Loading and Response for a Tall Building in the Non-Seismic Doldrums. Eng Struct 2005; 27(12): 1801–12.

[11] Kijewski-Correa T, Kochly M. Monitoring the wind-induced response of tall buildings: GPS performance and the issue of multipath effects. J Wind Eng Ind Aerod 2007; 95(9–11):1176–98.

[12] Park HS, Sohn HG, Kim IS, Park JH. Application of GPS to monitoring of wind-induced responses of high-rise buildings. Struct Des Tall Spec 2008; 17(1):117–32.

[13] Dalgliesh W A, Rainer J H. Measurements of wind induced displacements and accelerations of a 57 storey building in Toronto, Canada. Proceedings of the 3rd Colloquium on Industrial Aerodynamics 1978; Aachen, Germany.

[14] Isyumov N, Davenport AG, Montbaliu J. CN Tower, Toronto: model and full-scale response to wind. Proceedings of the 12th Congress, International Association for Bridge and Structural Engineering (IABSE) 1984; Vancouver, Canada, 737-46.

[15] He XF, Guang Y, Ding XL, Chen YQ. Application and evaluation of a GPS multi-antenna system for dam deformation monitoring. Earth Planets Space 2004; 56(11):1035–9.

[16] He XF, Sang W, Chen YQ, Ding XL. Steep slope monitoring: GPS multiple antenna system at Xiaowan Dam. GPS World 2005; 16(11):20–5.

[17] Cazzaniga NE, Pinto L, Forlani G, Abruzzi P. Monitoring oscillations of slender structures with GPS and accelerometers. In: Proc of the FIG Working Week 2005 and GSDI-8, Cairo, Egypt, 2005; 16–21.

[18] Li XJ, Ge LL, Ambikairajah E, Rizos C, Tamura Y, Yoshida A. Full-scale structural monitoring using an integrated GPS and accelerometer system. GPS Solut 2006; 10(4):233–47.

[19] Smyth A, Wu ML. Multi-rate Kalman filtering for the data fusion of displacement and

acceleration response measurements in dynamic system monitoring. Mech Syst Signal Pr 2007; 21(2):706–23.
[20] Psimoulis PA, Stiros SC. Experimental assessment of the accuracy of GPS and RTS for the determination of the parameters of oscillation of major structures. Compu-Aided Civ Inf 2008; 23(5):389–403.
[21] Yigit CO, Li XJ, Inal C, Ge L, Yetkin M. Preliminary evaluation of precise inclination sensor and GPS for monitoring full-scale dynamic response of a tall reinforced concrete building. J Appl Geodesy 2010; 4(2):103–13.
[22] Yi TH, Li HN, Gu M. Recent research and applications of GPS-based monitoring technology for high-rise structures. Struct Control Hlth 2013; 20:649-70.
[23] Chen WH, Lu ZR, Lin W, Chen SH, Ni YQ, Xia Y, Liao WY. Theoretical and experimental modal analysis of the Guangzhou New TV Tower. Eng Struct 2011; 33 (12): 3628-3646.
[24] Xia Y, Ni YQ, Zhang P, Liao WY, Ko JM. Stress Development of a Super-tall Structure during Construction: Field Monitoring and Numerical Analysis. Compu-Aided Civ Inf 2011; 26:542-99.
[25] Ni YQ, Wong KY, Xia Y. Health Checks through Landmark Bridges to Sky-high Structures. Adv Struct Eng 2011; 14(1):103-19.
[26] Xia Y, Xu YL, Wei ZL, Zhu HP, Zhou XQ. Variation of Structural Vibration Characteristics versus Non-uniform Temperature Distribution. Eng Struct 2011; 33 (1): 146-153.
[27] Geokon http://www.geokon.com/content/datasheets/4200_Series_Strain_Gages.pdf
[28] Geokon http://www.geokon.com/content/datasheets/4000_Strain_Gage.pdf
[29] Wolberg J. Data Analysis Using the Method of Least Squares: Extracting the Most Information from Experiments. Berlin Heidelberg New York: Springer-Verlag; 2006.
[30] Nickitopoulou A, Protopsalti K, Stiros S. Monitoring dynamic and quasi-static deformations of large flexible engineering structures with GPS: Accuracy, limitations and promises. Eng Struct 2008; 28 (10): 1471-1482.